UT DALLAS | Eugene McDermott Library

School of Natural Sciences and Mathematics

2012-7-30

Effects of Spherical Fullerene Nanoparticles on a Dipalmitoyl Phosphatidylcholine Lipid Monolayer: A Coarse Grain Molecular Dynamics Approach

Chi-cheng Chiu, *et al.*

PAPER

Effects of spherical fullerene nanoparticles on a dipalmitoyl phosphatidylcholine lipid monolayer: a coarse grain molecular dynamics approach†

Chi-cheng Chiu,‡[a] Wataru Shinoda,[b] Russell H. DeVane[c] and Steven O. Nielsen*[a]

The effect of carbon-based nanoparticles (CNPs) on biological systems is currently of great concern. Yet, few experimental techniques are capable of directly imaging and probing the energetics of such nano-bio systems. Here, we use coarse grain molecular dynamics simulations to study spherical fullerene molecules interacting with dipalmitoyl phosphatidylcholine (DPPC) lipid membranes. Using free energy calculations we show that all the tested fullerene molecules can spontaneously diffuse into both a lipid bilayer and a lipid monolayer. In addition, we establish that large fullerene molecules tend to partition preferentially into bilayers, which affects the lipid monolayer-to-bilayer transition during the respiration cycle. Our results identify a possible CNP perturbation to the function of the pulmonary monolayer membrane and suggest a potential pathway for CNP entry into the body through lung inhalation.

1 Introduction

Carbon-based nanoparticles (CNPs), such as spherical fullerenes and carbon nanotubes, have many potential applications in nanoelectronics, energy conservation devices, cancer therapy, drug delivery, and biological sensors due to their unique mechanical and electronic properties.[1,2] With increasing interest in CNPs in science and industry, the environmental, safety, and health (ESH) concerns of CNPs have recently been a focus of attention.[2]

One route of exposure to CNPs is through lung inhalation.[3–5] In human lungs, the alveolus inner surface contains the lung surfactant monolayer (or pulmonary surfactant monolayer) which reduces the air/water surface tension and prevents the lungs from collapsing at the end of expiration. In the 1950s it was found that respiratory distress syndrome in premature infants is caused by a lack of pulmonary surfactant and it is now established clinical practice to treat this disease by using exogenous

[a] Department of Chemistry, The University of Texas at Dallas, 800 West Campbell Road, Richardson, TX 75080, USA. E-mail: steven.nielsen@utdallas.edu; Fax: +1-(972)-883-2925; Tel: +1-(972)-883-5323
[b] Nanosystem Research Institute, National Institute of Advanced Industrial Science and Technology (AIST), Central 2, Umezono 1-1-1, Tsukuba, 305-8568, Japan
[c] Corporate R&D, Modeling and Simulation, The Procter and Gamble Company, Cincinnati, OH 45069, USA
† Electronic supplementary information (ESI) available. See DOI: 10.1039/c2sm26357b
‡ Present address: Chemical and Biological Engineering Department, The University of Wisconsin-Madison, 1415 Engineering Drive, Madison, WI 53706, USA.
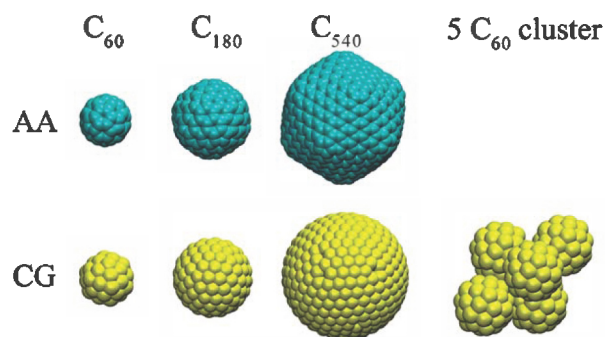
surfactant preparations.[6] Lung surfactants (LS) include proteins, cholesterol, and various phospholipids.[7,8] Numerous experimental (both *in vivo* and *in vitro*) and computational studies have been conducted to investigate the surface properties, structure, and function of the pulmonary monolayer.[8–21] It has been shown that the alveolus inner surface includes multiple lipid bilayer stacks[12,13] which are stabilized by surfactant proteins (SP-B and SP-C) and connected with the pulmonary monolayer.[8–10] During the respiration cycle, the lung alveoli surface expands and contracts which leads to the expansion/compression of the pulmonary monolayer. During compression, the excess lipid molecules leave the monolayer and are stored in the bilayer stacks located just below the monolayer in the fluid phase; lipids then cycle back to the monolayer during expansion. The cycling of lipid molecules between the monolayer and bilayer stacks is regulated by the surfactant proteins. All-atom molecular dynamics (AAMD) simulations have been used to understand the interactions between the surfactant proteins and the lipid monolayer.[17–19] More recently, Baoukina *et al.* utilized coarse grain molecular dynamics (CGMD) to explore the molecular mechanism of the pulmonary monolayer collapse and transformation into bilayer structures during the respiration cycle.[20,21]

Nanoparticles present in the atmosphere, through inhalation, can interact with the inner surface of the lung alveoli.[3–5] The toxicity of CNPs, according to various experimental results, remains disputable.[22–34] This controversy is partly due to the variation of the CNP size, shape, functionalization, and aggregation state in different experiments.[35,36] Huczko *et al.* reported minor toxicity of CNPs towards lung tissue.[22] Yang *et al.* showed that C_{60} has minor effects on the monolayer surface properties,

e.g. the surface tension/area isotherm.[23] On the other hand, *in vivo* tests using mice have shown that CNPs can induce airway fibrosis and granulomas in the lung,[24,25] although a very recent study concluded that the toxicity is attributable to CNP aggregation.[34] To gain an understanding of the bio-activity of CNPs at the molecular level, Violi *et al.* used AAMD to study the effect of airborne CNPs on the pulmonary monolayer.[37] Their results showed that CNPs can easily penetrate the monolayer and may affect interactions between the LS proteins and the LS phospholipids. Further translocation of CNPs into the water phase was found to be unfavorable.

In this study, we used CGMD to investigate the effect of spherical fullerene molecules on a dipalmitoyl phosphatidylcholine (DPPC) lipid monolayer, which is a model pulmonary surfactant monolayer. From the CNP family we chose to focus on spherical fullerenes and assessed how different sizes of fullerenes impact the lipid monolayer-to-bilayer transition during the respiration cycle. Our results show that large fullerenes strongly perturb the lipid monolayer-to-bilayer transformation energetics.

2 Methods

2.1 Fullerene model

Fullerene molecules were constructed from the CG benzene site (BER) developed by DeVane *et al.*[38–40] This representation has previously been applied to study the effect of spherical fullerenes on a lipid bilayer.[40,41] In this study, the fullerene molecules we focused on were C_{60}, C_{180}, and C_{540}. With the CG : AA carbon mapping ratio of 2 : 3 for the BER site, CG C_{60}, C_{180}, and C_{540} molecules contain 40, 120, and 360 interaction sites, respectively. We placed 40 BER beads on a spherical surface of radius 0.35 nm for C_{60}, 120 BER beads on a 0.61 nm radius spherical surface for C_{180}, and 360 BER beads on a 1.05 nm radius spherical surface for C_{540}. Each fullerene CG representation was relaxed through energy minimization with the BER beads constrained to the spherical surface. The resulting energy-minimized structure for the CG fullerene was subsequently treated as a rigid body in the MD studies using the rigid module in LAMMPS which precludes intramolecular bond and angle potentials.[42] Fig. 1 illustrates the molecular structure of the three fullerene molecules and their corresponding CG representations.

Fig. 1 All atom structures (top row) and coarse grain representations (bottom row) of the fullerene molecules C_{60}, C_{180}, and C_{540} used in this study. The bottom right figure displays a representative geometry of the 5-membered C_{60} cluster used to study the effect of C_{60} aggregates on lipid monolayers.

2.2 Lipid monolayer model

One important feature of the lung surfactant (LS) monolayer is to reduce the surface tension at the air–water interface. The actual lung surfactant (LS) monolayer is a complex mixture of protein, cholesterol, and phospholipids, wherein DPPC is the major component. The interaction between fullerenes and LS molecules thus requires consideration of fullerene–lipid, fullerene–protein, and fullerene–cholesterol interactions among others. To approach such a complex system, we began in this study with a DPPC monolayer. Studies with multiple LS components will be reported in the future. The CG model for a DPPC monolayer developed by Shinoda *et al.* has been shown to reproduce the experimental surface tension *versus* area per lipid isotherm.[43] In addition, from the same study, a simulation of an oversaturated DPPC monolayer with an initial area per lipid of 0.4 nm^2 showed the spontaneous formation of a bicelle, indicating the ability of the model to study the monolayer to bilayer transition in the absence of the protein, cholesterol, and other LS components.
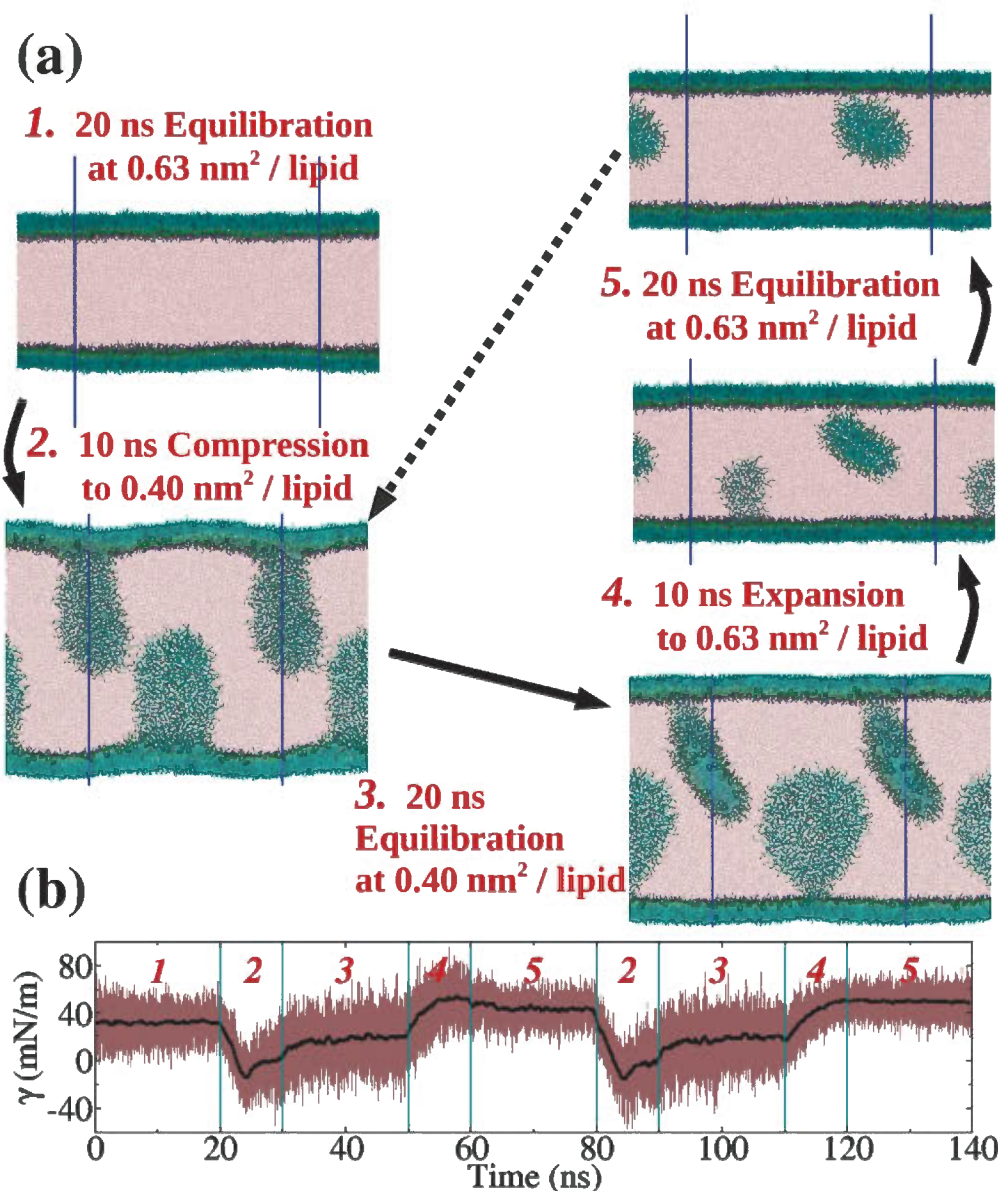
2.3 Molecular dynamics simulation

CGMD simulations were performed using the LAMMPS MD package.[42] All CG simulations were carried out using a two level RESPA multi-time step integrator.[44] The bond and angle potentials were evaluated in the inner timestep of 2 fs, and the non-bonded interactions, including van der Waals and electrostatic interactions, were evaluated in the outer timestep of 20 fs. The van der Waals and the short range electrostatic interactions were truncated at 15 Å. The long range Coulomb interactions were calculated *via* standard Ewald summation implemented in the LAMMPS package with the maximum root mean square error of 1×10^{-4} in the per-atom forces.[45] The Nosé–Hoover algorithm was used to control the temperature with the damping factor of 100 fs and the pressure with the damping factor of 1000 fs.[46] The CG models for water and DPPC molecules were taken from the CG force field developed by Shinoda *et al.*,[43,47] and the interactions involving the BER site used the parameters developed by DeVane *et al.*[38–40]

For equilibrium studies, the DPPC monolayer system was composed of a water slab with two water–vacuum interfaces protected by two symmetric DPPC monolayers normal to the *z* direction. The system included 84 000 water CG sites (equivalent to 252 000 water molecules) and 2048 DPPC molecules (1024 DPPC per monolayer) in a simulation unit cell of size $25.3 \times 25.3 \times 40.0$ nm^3. This corresponds to an average area per lipid of 0.63 nm^2 (62.5 Å^2) with a surface tension of ≈ 31 mN m^{-1}.[43] The box *z* dimension (L_z) was set to 40.0 nm to minimize the interaction between the system and its periodic images. For the fullerene–DPPC monolayer systems, fullerene molecules were inserted into the vacuum phase 1.5–2.5 nm from the DPPC monolayer (measured between the centers of mass of the fullerene and the DPPC monolayer). To study the effect of the C_{60} concentration, we tested 5, 10, and 20 C_{60} molecules per monolayer, which correspond to [C_{60}]/[DPPC] molar ratios of 4.9×10^{-3}, 9.8×10^{-3}, and 2.0×10^{-2}, respectively. In our previous studies, we showed that C_{60} aggregates in both a hydrocarbon melt and a lipid bilayer, which is also expected here

in the hydrophobic interior of the lipid monolayer.[39,40] However, such aggregation depends on the diffusion of C_{60}, and a long equilibrium simulation (>100 ns) is thus required.[39,40] Hence, in this study, we started with four 5-membered C_{60} clusters (Fig. 1), equivalent to a $[C_{60}]/[DPPC]$ molar ratio of 2.0×10^{-2}, to study the influence of C_{60} aggregates. The size of the 5-membered C_{60} cluster (with an average radius of 0.74 nm) is between the sizes of C_{180} and C_{540}. No constraints were applied to maintain the integrity of the cluster during the simulation. For C_{180} and C_{540}, we tested 10 fullerene molecules per monolayer, namely a $[fullerene]/[DPPC]$ molar ratio of 9.8×10^{-3}, and compared with the C_{60} systems to study the effect of fullerene size. All systems was equilibrated at 323 K under the NVT ensemble for 20 ns.

To investigate the lipid monolayer to bilayer transformation during the respiration cycle, we laterally compressed the monolayer system to decrease the average area per lipid to 0.40 nm^2 leading to a negative surface tension and monolayer collapse. Fig. 2 illustrates the process of (1) system equilibration at 0.63 nm^2 per lipid, (2) compression to 0.40 nm^2 per lipid, and (3) re-equilibration of the system at 0.40 nm^2 per lipid. The compression (step 2) was done by changing the box x- and y-dimensions, L_x and L_y, at a constant rate of 0.51 nm ns^{-1} for 10 ns. We also tested the compression rates of 0.051, 0.255, 0.51, and 5.1 nm ns^{-1}. All compression rates give similar results as to the monolayer collapse and surface energy change (data not shown). This is consistent with the study by Baoukina et al. who

Fig. 2 (a) The compression–expansion cycle used to study the lipid monolayer–bilayer transition: (1) the system first was equilibrated at 0.63 nm^2 per lipid for 20 ns; then (2) compressed in the lateral dimensions for 10 ns to 0.40 nm^2 per lipid; (3) the system was then equilibrated for 20 ns at 0.40 nm^2 per lipid; (4) for certain fullerene–monolayer systems, the system was further re-expanded for 10 ns back to 0.63 nm^2 per lipid and (5) re-equilibrated for 20 ns. (b) The time evolution of the surface tension for a pure DPPC monolayer system during each step in two consecutive compression–expansion cycles. The surface tension measured every 2 ps is plotted in pink. The black line shows the running average of every 200 data points.

reported that the pathway of monolayer collapse was independent of the monolayer composition, compression method, and rate.[21] For computational efficiency, we chose the compression rate of 0.51 nm ns^{-1} for all the monolayer systems. After compression, the system was relaxed and equilibrated at 0.40 nm^2 per lipid for 20 ns under the NVT ensemble (step 3). For certain monolayer systems, after equilibration at 0.40 nm^2 per lipid, the systems were expanded back to 0.63 nm^2 per lipid at the same rate of 0.51 nm ns^{-1} in the x- and y-dimensions for 10 ns (step 4), and then equilibrated for 20 ns (step 5) to test the reversibility of the monolayer compression.

2.4 Free energy calculations

The free energy profile of a fullerene transferring across the lipid monolayer was calculated using the umbrella sampling technique combined with the weighted histogram analysis method (WHAM).[48] The monolayer system used for the free energy calculations contained 512 DPPC molecules and 21 000 water CG sites within a simulation unit cell of $12.7 \times 12.7 \times 40.0$ nm^3, which was a quarter of the system size used in the equilibrium studies. The transfer free energy profile was evaluated as a function of the z-distance between the centers of mass of the fullerene and the lipid monolayer. Sampling windows were deployed every 0.4 nm in the z-direction, each with an applied harmonic biasing potential of force constant 209.2 kJ mol^{-1} nm^{-2}. Each sampling window was simulated under the NVT ensemble at 323 K for 40 ns. The initial configuration of each sampling window was extracted from one of two equilibrium trajectories where the fullerene was placed in vacuum or in the aqueous phase as the starting configurations. The error of the free energy profiles was estimated via the bootstrap method.[49] Considering the system with the largest fullerene (C_{540}) and assuming a C_{540} cross-section of πr^2, where r is the radius of C_{540}, we may estimate that the area per lipid changes from 0.63 nm^2 to 0.62 nm^2 after C_{540} insertion into the monolayer, which is considered to have a limited effect on the free energy calculation.

For comparison, we also computed the transfer free energy of a fullerene for a DPPC bilayer system. The bilayer system contained 512 DPPC molecules and 20 500 water CG beads in a $12.7 \times 12.7 \times 15.6$ nm^3 simulation unit cell which corresponds to an average of 0.63 nm^2 per lipid and a total system surface tension of near zero.[43] The sampling windows and the corresponding biasing potentials were the same as for the monolayer system. The initial configuration of each sampling window, similar to the monolayer system, was extracted from an equilibrium trajectory with the fullerene placed in the aqueous phase as the starting configuration. Each sampling simulation of the lipid bilayer system was performed for 40 ns under the NP$_{xy}$T ensemble at 1 atm and 323 K where the x- and y-dimensions of the simulation box are coupled and the z-dimension dilates and contracts independently. The convergence of the free energy profiles is shown in the ESI.†

3 Results and discussion

3.1 Effect of fullerenes on a DPPC monolayer

We performed 20 ns equilibrium simulations of DPPC monolayer systems with [fullerene]/[DPPC] molar ratios of 4.9×10^{-3},

9.8×10^{-3}, and 2.0×10^{-2} for C_{60}, and of 9.8×10^{-3} for C_{180} and C_{540}. The surface tension of each monolayer is calculated by

$$\gamma = \frac{L_z}{2}\left(\langle P_{zz} \rangle - \frac{\langle P_{xx} + P_{yy} \rangle}{2} \right) \qquad (1)$$

where P_{xx}, P_{yy}, P_{zz} are the diagonal pressure tensor components, the angle brackets indicate the time average, L_z is the z-dimension of the simulation box, and the first factor of 1/2 is due to the two monolayers in the system. The error is evaluated using the block-averaging method.[50] As shown in Fig. 3, the surface tension slightly increases with the C_{60} concentration, from 31 mN m^{-1} for pure DPPC to 32 mN m^{-1} for [C_{60}]/[DPPC] = 2.0×10^{-2}. The small effect of C_{60} on the surface tension agrees with the experimental results reported by Wang and Yang.[23] On the other hand, C_{60} clusters, each with an average radius of 0.74 nm, have a larger effect on the surface tension compared with dispersed C_{60} of the same concentration ([C_{60}]/[DPPC] = 2.0×10^{-2}). This may be due to the large size of the C_{60} aggregate so that DPPC molecules cannot fully cover the fullerene surface leading to an exposure of the C_{60} surface to the vacuum or water phases. Such size effects can also be seen by comparing the surface tension of C_{60}, C_{180}, and C_{540} doped DPPC monolayers. For C_{180} (radius = 0.61 nm), the surface tension is similar to C_{60} of the same fullerene concentration. For C_{540} (radius = 1.05 nm), the fullerene can no longer be entirely contained within the lipid monolayer which results in partial exposure of the C_{540} molecules to the water or vacuum phases. In addition, the large size of C_{540} causes a decrease in the effective area per lipid molecule. Assuming a C_{540} cross-section of πr^2, where r is the radius of C_{540}, we can roughly estimate that, for the [C_{540}]/[DPPC] = 9.8×10^{-3} monolayer system, the area per lipid is reduced to 0.59 nm^2. The overall surface tension of the C_{540}–DPPC monolayer system includes the interfacial tensions of the lipid–water, lipid–vacuum, C_{540}–water, and C_{540}–vacuum interfaces. The resulting system surface tension is much lower than for C_{60} or C_{180} doped monolayer systems with the same fullerene concentration.
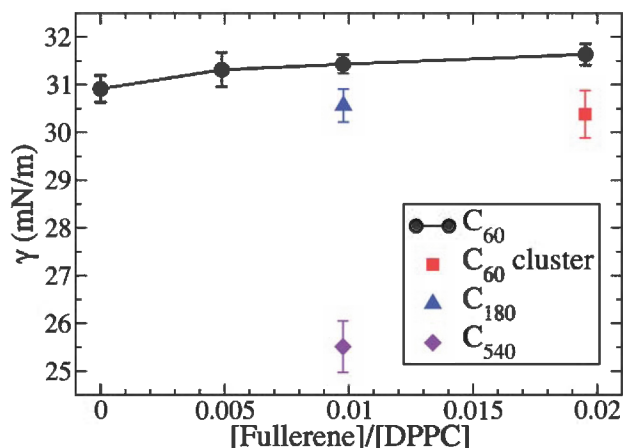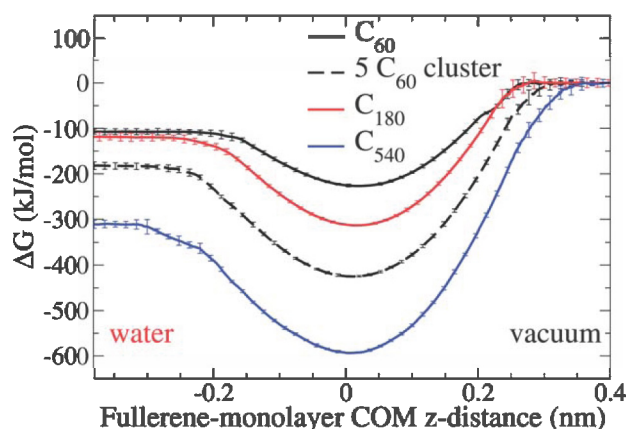

Fig. 3 The surface tension of the monolayer as a function of the fullerene concentration. Monolayers doped with C_{60} and the C_{60} cluster are plotted with circles and a square, respectively. The systems containing C_{180} and C_{540} are represented using a triangle and a diamond, respectively.
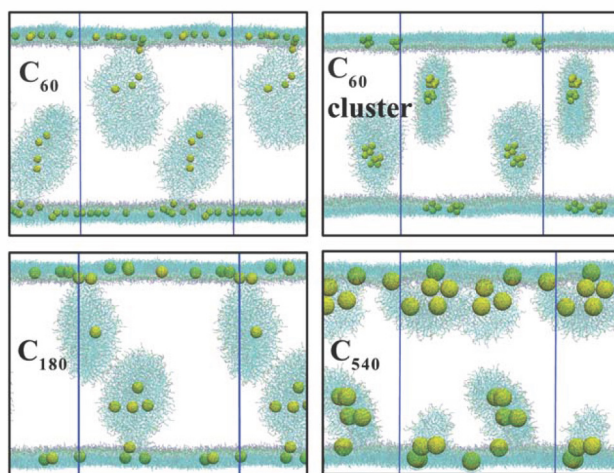
Fig. 4 The free energy profile of transferring fullerene molecules from the vacuum phase ($z > 0$) into the water phase ($z < 0$) as a function of the center of mass z-distance between the fullerene and the DPPC monolayer. Profiles for C_{60} and the 5-membered C_{60} cluster are plotted using the black solid and black dashed lines, respectively. Profiles for C_{180} and C_{540} are plotted using red and blue lines, respectively.
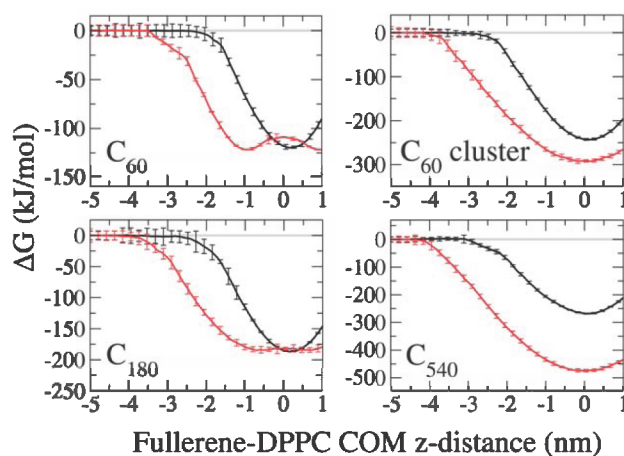

Fig. 5 The snapshots of the system configurations at the end of the step 3 equilibration shown in Fig. 2 for DPPC monolayer systems doped with C_{60} (top left panel), C_{60} clusters (top right panel), C_{180} (bottom left panel), and C_{540} (bottom right panel).

Fig. 4 illustrates the free energy profiles of transferring fullerene molecules from vacuum, through the DPPC monolayer, into the water phase. All tested fullerenes show a propensity to partition into the DPPC monolayer suggesting their spontaneous diffusion into the membrane. Also, the interaction between the fullerene and the DPPC monolayer increases with the fullerene size. For a 5-membered C_{60} cluster, we observed a greater free energy change compared with a C_{60} molecule. The more favorable interaction free energy with the monolayer for the large fullerene sizes can be correlated to the decrease in overall surface tension as shown in Fig. 3. If we view the water–vacuum interface with the DPPC monolayer as a simple liquid–vacuum interface, the greater free energy changes for larger fullerene sizes can be interpreted as the result of a larger removal of liquid–vacuum interface in analogy to Pieranski's derivation of the interfacial localization of particles.[51]

3.2 DPPC monolayer to bilayer transition

Fig. 2 displays snapshots of a pure DPPC monolayer system at the end of each step of the compression–expansion cycle. After compressing an equilibrated system from 0.63 nm^2 to 0.40 nm^2 per lipid (step 2), the DPPC monolayer buckles and starts to form a bicelle structure – a disk-like, bilayered lipid micelle. After 20 ns of equilibration (step 3), two bicelles from the two interfaces are nearly detached from the DPPC monolayer. Upon re-expanding the compressed system back to 0.63 nm^2 per lipid and equilibrating for 20 ns, one of the bicelles fuses back into the DPPC monolayer whereas the other one remains detached from the monolayer. The system surface tension converges at the end of each equilibration step indicating the system interfacial energy is equilibrated. In the actual pulmonary surfactant layer in lung alveoli, proteins are needed to connect the bilayer lamella with the monolayer and assist in transporting the lipids back to the monolayer during the respiration cycle.[8,17–21] However, the monolayer system studied here contains only DPPC molecules, and thus a bicelle cannot easily fuse back into the monolayer if it detaches as seen in Fig. 2.

Similar compressions were conducted on the systems with [fullerene]/[DPPC] molar ratios of 2.0×10^{-2} for C_{60} and 5-membered C_{60} clusters, and 9.8×10^{-3} for C_{180} and C_{540}. Fig. 5 shows the snapshots for each system after equilibration of the compressed systems (step 3 in Fig. 2). For the monolayer systems doped with C_{60}, C_{60} clusters, and C_{180}, one large bicelle was formed from each monolayer after the compression as seen in the pure DPPC system. Fullerene molecules were observed inside each bicelle. For the C_{540} doped DPPC monolayer, multiple small bicelle structures containing C_{540} molecules were formed instead of one large bicelle, indicating a strong perturbation of the lipid monolayer–bilayer transition.

3.3 Fullerene partitioning between monolayer and bilayer structures
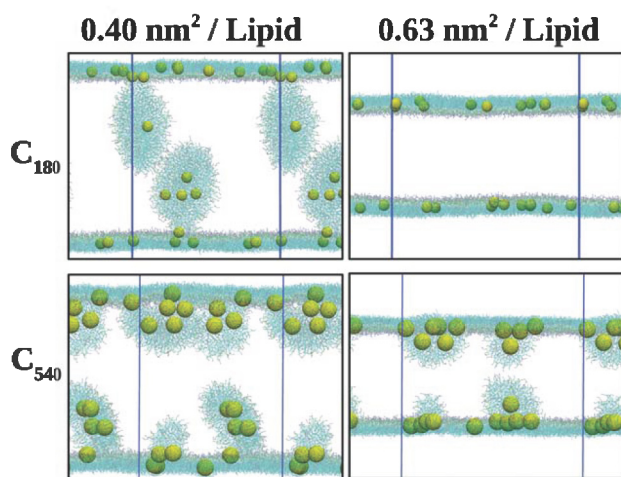
To study the effect of fullerene molecules on the DPPC monolayer–bilayer transition, we calculated the free energy profile of transferring a fullerene molecule from water into a DPPC bilayer and compared with the monolayer system. The resulting free energy profiles for C_{60}, a 5-membered C_{60} cluster, C_{180}, and C_{540} are shown in Fig. 6. For C_{60}, the transfer free energy minimum value for the DPPC monolayer ($\Delta G_{mono} = -117$ kJ mol^{-1}) is very close to that for the bilayer ($\Delta G_{bilayer} = -121$ kJ mol^{-1}). Similarly in the C_{180} systems, the monolayer ΔG_{mono} is -184 kJ mol^{-1}, close to $\Delta G_{bilayer}$ of -184 kJ mol^{-1}. These free energy values suggest that there is no preference for C_{60} or C_{180} to partition in the monolayer *versus* the bilayer system. In the case of the C_{60} cluster, however, $\Delta G_{bilayer}$ is -293 kJ mol^{-1}, which is more favorable than $\Delta G_{mono} = -247$ kJ mol^{-1}. This suggests that C_{60} clusters prefer being in a DPPC bilayer *versus* a monolayer. The difference in the water–membrane transfer free energy between the monolayer and the bilayer systems is particularly large for C_{540} where $\Delta G_{bilayer} = -473$ kJ mol^{-1} compared with $\Delta G_{mono} = -268$ kJ mol^{-1}. This indicates that C_{540} molecules have a strong tendency to partition into a lipid bilayer *versus* a lipid monolayer. This also suggests that C_{540} molecules can induce lipid bilayer formation during the system

Fig. 6 Transfer free energy profiles from water into a monolayer (black) or a bilayer (red) for a C_{60} molecule (top left), a 5-membered C_{60} cluster (top right), a C_{180} molecule (bottom left), and a C_{540} molecule (bottom right).

lateral compression; this results in multiple bicelles formed from a monolayer system which is different from the behavior of the other fullerene doped monolayer systems we studied where only one large bicelle is formed during the compression as illustrated in Fig. 5.

To further study the bilayer inducing effect of C_{540}, we expanded the compressed C_{540}–DPPC monolayer system, as shown in Fig. 5, from 0.40 nm² per lipid back to 0.63 nm² per lipid in a 10 ns period and then equilibrated the system for 20 ns (step 4 and 5 in Fig. 2). In comparison, we also conducted the same expansion/equilibration on the compressed C_{180}–DPPC monolayer system. Fig. 7 displays the system configurations at the end of equilibration. For C_{180}, the bicelle formed from each monolayer fuses back into the monolayer after the expansion. Yet, for C_{540}, due to the large preference of C_{540} for lipid bilayers, the bicelles do not fully fuse back into the monolayer but rather

Fig. 7 The snapshots illustrate the system configurations at the end of 20 ns of equilibration at 0.40 nm² per lipid (step 3 in Fig. 2, shown in the left column) compared with that at the end of 20 ns of equilibration after re-expansion back to 0.63 nm² per lipid (step 5 in Fig. 2, shown in the right column). The monolayer systems doped with C_{180} and C_{540} are shown in the top row and the bottom row, respectively.

form hemi-spherical buds around C_{540} molecules creating a local bilayer-like environment. The failure of the bicelles to fuse back with the monolayer observed for the C_{540} system is intrinsically different from what is observed in the pure DPPC system (Fig. 2). In the pure DPPC system, the bicelle fails to fuse back due to its complete detachment from the monolayer; fusion in this case would be an activated process requiring lipid reorganization. For the C_{540} system, the bicelles remain attached to the monolayer during the compression–expansion cycle. The preferential solvation of the C_{540} particles in a local bilayer-like lipid environment prevents the lipids from flowing back into the monolayer during the expansion cycle. After the expansion, roughly 15 out of the 20 C_{540} molecules localized in the hemi-spherical micelles or at the micelle/monolayer junctions. As a result, there are fewer lipid molecules in the monolayer, and the final surface tension for the C_{540}–monolayer system after the compression–expansion cycle is 49.5 mN m⁻¹, much higher than 25.6 mN m⁻¹ before the cycle. This surface energy change is compensated by the large free energy difference of C_{540} in the bilayer *versus* the monolayer. This suggests that the presence of C_{540} may strongly perturb the lipid monolayer–bilayer transition during the respiration cycle in the lung alveoli.

In the actual LS monolayer system, due to the presence of proteins and other LS components, the detailed mechanism of the monolayer–bilayer transformation may differ from the model system used in the present study. However, the free energy data suggests an equal partitioning of C_{60} and C_{180} between the monolayer and the bilayer, and a preferential partitioning of C_{540} toward the bilayer system. The combined results suggest that, after lung inhalation, one possible entry mechanism for fullerenes into the body is initiated by the lipid monolayer–bilayer transition.

4 Conclusions

We performed coarse grain molecular dynamics simulations to study the effect of different sized fullerene molecules on a DPPC monolayer system. For all the concentrations tested ([C_{60}]/[DPPC] = 0 to 0.02), C_{60} has little influence on the surface tension of the monolayer system in agreement with the experimental data reported by Wang and Yang.[23] Similarly, for the 5-membered C_{60} cluster and C_{180}, small effects were found on the system surface tension. However, for a large fullerene such as C_{540}, the particle size is too large to fully submerge inside the monolayer leading to partial exposure of C_{540} to the air and water phases. The resulting system surface tension is much reduced from a pure DPPC monolayer.

We also laterally compressed/expanded the DPPC monolayer system to study the monolayer–bilayer transition. After compression, for C_{60}, the C_{60} cluster, and C_{180} doped DPPC monolayers, we observed the collapse-induced formation of one large bicelle structure from each monolayer; fullerene molecules are included in the budded bicelles. For the C_{180}–DPPC system, the bicelle fuses back into the monolayer after re-expanding. In the case of the C_{540} doped DPPC monolayer, multiple small bicelles containing C_{540} molecules were formed after lateral compression. These small bicelles did not fuse back into the monolayer after re-expansion of the system. According to our free energy data, C_{540} preferentially partitions inside a lipid

bilayer *versus* a monolayer. The strong preference of C_{540} towards a lipid bilayer results in the observed perturbation of the monolayer–bilayer transition.

The combined results suggest that, during the monolayer–bilayer transition, fullerene molecules can leave the air–water interface by partitioning into the bilayer structure formed from the monolayer collapse. Large sized fullerene particles show a strong preference to partition into a bilayer which strongly affects the monolayer–bilayer transition. The molecular mechanism revealed in this work has implications for the size effect of fullerene on the lung surfactant system. Future studies include expanding to other CNPs, such as carbon nanotubes and airborne nanoparticles, and also to a more complex lung surfactant system containing cholesterol and surfactant proteins.

References

1 R. H. Baughman, A. A. Zakhidov and W. A. de Heer, *Science*, 2002, **297**, 787–792.
2 C. Buzea, I. I. Pacheco and K. Robbie, *Biointerphases*, 2007, **2**, MR17–MR71.
3 G. Oberdorster, Z. Sharp, V. Atudorei, A. Elder, R. Gelein, A. Lunts, W. Kreyling and C. Cox, *J. Toxicol. Environ. Health, Part A*, 2002, **65**, 1531–1543.
4 J. W. Card, D. C. Zeldin, J. C. Bonner and E. R. Nestmann, *Am. J. Physiol.*, 2008, **295**, L400–L411.
5 J. J. Li, S. Muralikrishnan, C. T. Ng, L. Y. L. Yung and B. H. Bay, *Exp. Biol. Med.*, 2010, **235**, 1025–1033.
6 J. Johansson and T. Curstedt, *Eur. J. Biochem.*, 1997, **244**, 675–693.
7 R. Wustneck, J. Perez-Gil, N. Wustneck, A. Cruz, V. B. Fainerman and U. Pison, *Adv. Colloid Interface Sci.*, 2005, **117**, 33–58.
8 J. Perez-Gil, *Biochim. Biophys. Acta, Biomembr.*, 2008, **1778**, 1676–1695.
9 S. Schurch, R. Qanbar, H. Bachofen and F. Possmayer, *Biol. Neonate*, 1995, **67**, 61–76.
10 H. J. Galla, N. Bourdos, A. von Nahmen, M. Amrein and M. Sieber, *Thin Solid Films*, 1998, **327**, 632–635.
11 S. T. Milner, J. F. Joanny and P. Pincus, *Europhys. Lett.*, 1989, **9**, 495–500.
12 A. vonNahmen, M. Schenk, M. Sieber and M. Amrein, *Biophys. J.*, 1997, **72**, 463–469.
13 M. M. Lipp, K. Y. C. Lee, D. Y. Takamoto, J. A. Zasadzinski and A. J. Waring, *Phys. Rev. Lett.*, 1998, **81**, 1650–1653.
14 W. X. Lu, C. M. Knobler, R. F. Bruinsma, M. Twardos and M. Dennin, *Phys. Rev. Lett.*, 2002, **89**, 146107.
15 C. Ybert, W. X. Lu, G. Moller and C. M. Knobler, *J. Phys. Chem. B*, 2002, **106**, 2004–2008.
16 J. Saccani, S. Castano, F. Beaurain, M. Laguerre and B. Desbat, *Langmuir*, 2004, **20**, 9190–9197.
17 J. A. Freites, Y. Choi and D. J. Tobias, *Biophys. J.*, 2003, **84**, 2169–2180.
18 S. K. Kandasamy and R. G. Larson, *Biophys. J.*, 2005, **88**, 1577–1592.
19 H. Lee, S. K. Kandasamy and R. G. Larson, *Biophys. J.*, 2005, **89**, 3807–3821.
20 S. Baoukina, L. Monticelli, M. Amrein and D. P. Tieleman, *Biophys. J.*, 2007, **93**, 3775–3782.
21 S. Baoukina, L. Monticelli, H. J. Risselada, S. J. Marrink and D. P. Tieleman, *Proc. Natl. Acad. Sci. U. S. A.*, 2008, **105**, 10803–10808.
22 A. Huczko, H. Lange, E. Calko, H. Grubek-Jaworska and P. Droszcz, *Fullerene Sci. Technol.*, 2001, **9**, 251–254.
23 Z. N. Wang and S. H. Yang, *ChemPhysChem*, 2009, **10**, 2284–2289.
24 J. P. Ryman-Rasmussen, M. F. Cesta, A. R. Brody, J. K. Shipley-Phillips, J. I. Everitt, E. W. Tewksbury, O. R. Moss, B. A. Wong, D. E. Dodd, M. E. Andersen and J. C. Bonner, *Nat. Nanotechnol.*, 2009, **4**, 747–751.
25 J. P. Ryman-Rasmussen, E. W. Tewksbury, O. R. Moss, M. F. Cesta, B. A. Wong and J. C. Bonner, *Am. J. Respir. Cell Mol. Biol.*, 2009, **40**, 349–358.
26 K. Donaldson, R. Aitken, L. Tran, V. Stone, R. Duffin, G. Forrest and A. Alexander, *Toxicol. Sci.*, 2006, **92**, 5–22.
27 C. A. Poland, R. Duffin, I. Kinloch, A. Maynard, W. A. H. Wallace, A. Seaton, V. Stone, S. Brown, W. MacNee and K. Donaldson, *Nat. Nanotechnol.*, 2008, **3**, 423–428.
28 C. W. Lam, J. T. James, R. McCluskey and R. L. Hunter, *Toxicol. Sci.*, 2004, **77**, 126–134.
29 D. B. Warheit, B. R. Laurence, K. L. Reed, D. H. Roach, G. A. M. Reynolds and T. R. Webb, *Toxicol. Sci.*, 2004, **77**, 117–125.
30 A. D. Maynard, P. A. Baron, M. Foley, A. A. Shvedova, E. R. Kisin and V. Castranova, *J. Toxicol. Environ. Health, Part A*, 2004, **67**, 87–107.
31 A. A. Shvedova, V. Castranova, E. R. Kisin, D. Schwegler-Berry, A. R. Murray, V. Z. Gandelsman, A. Maynard and P. Baron, *J. Toxicol. Environ. Health, Part A*, 2003, **66**, 1909–1926.
32 G. Oberdorster, J. Ferin and B. E. Lehnert, *Environ. Health Perspect.*, 1994, **102**, 173–179.
33 R. K. Harishchandra, M. Saleem and H.-J. Galla, *J. R. Soc., Interface*, 2010, **7**, S15–S26.
34 G. M. Mutlu, G. R. S. Budinger, A. A. Green, D. Urich, S. Soberanes, S. E. Chiarella, G. F. Alheid, D. R. McCrimmon, I. Szleifer and M. C. Hersam, *Nano Lett.*, 2010, **10**, 1664–1670.
35 A. Magrez, S. Kasas, V. Salicio, N. Pasquier, J. W. Seo, M. Celio, S. Catsicas, B. Schwaller and L. Forro, *Nano Lett.*, 2006, **6**, 1121–1125.
36 A. Nel, T. Xia, L. Madler and N. Li, *Science*, 2006, **311**, 622–627.
37 S. Choe, R. Chang, J. Jeon and A. Violi, *Biophys. J.*, 2008, **95**, 4102–4114.
38 R. DeVane, M. L. Klein, C.-c. Chiu, S. O. Nielsen, W. Shinoda and P. B. Moore, *J. Phys. Chem. B*, 2010, **114**, 6386–6393.
39 C.-c. Chiu, R. DeVane, M. L. Klein, W. Shinoda, P. B. Moore and S. O. Nielsen, *J. Phys. Chem. B*, 2010, **114**, 6394–6400.
40 R. DeVane, A. Jusufi, W. Shinoda, C.-c. Chiu, S. O. Nielsen, P. B. Moore and M. L. Klein, *J. Phys. Chem. B*, 2010, **114**, 16364–16372.
41 A. Jusufi, R. H. DeVane, W. Shinoda and M. L. Klein, *Soft Matter*, 2011, **7**, 1139–1146.
42 S. Plimpton, *J. Comput. Phys.*, 1995, **117**, 1–19.
43 W. Shinoda, R. DeVane and M. L. Klein, *J. Phys. Chem. B*, 2010, **114**, 6836–6849.
44 M. Tuckerman, B. J. Berne and G. J. Martyna, *J. Chem. Phys.*, 1992, **97**, 1990–2001.
45 M. P. Allen and D. J. Tildesley, *Computer Simulations of Liquids*, University Press, Oxford, 1992.
46 W. G. Hoover, *Phys. Rev. A*, 1985, **31**, 1695–1697.
47 W. Shinoda, R. Devane and M. L. Klein, *Mol. Simul.*, 2007, **33**, 27–36.
48 S. Kumar, D. Bouzida, R. H. Swendsen, P. A. Kollman and J. M. Rosenberg, *J. Comput. Chem.*, 1992, **13**, 1011–1021.
49 M. R. Chernick, *Bootstrap Methods: A Guide for Practitioners and Researchers*, Wiley-Interscience, New York, 2007.
50 H. Flyvbjerg and H. G. Petersen, *J. Chem. Phys.*, 1989, **91**, 461–466.
51 P. Pieranski, *Phys. Rev. Lett.*, 1980, **45**, 569–572.